ADVANCED FUNCTIONAL MATERIALS
www.afm-journal.de

Structure, Function, and Application of Self-Healing Adhesives from Mistletoe Viscin

*Stephen D. George, Elias Andraos, Tobias Priemel, Nils Horbelt, Griffin Keiser, Ambrish Kumar, Christian Heiss, Notburga Gierlinger, Parastoo Azadi, and Matthew J. Harrington**

Berries from the European Mistletoe (*Viscum album*) possess a sticky tissue called viscin that facilitates adhesion and germination onto host trees. Recent studies of viscin have demonstrated its adhesive capacity on a range of natural and synthetic surfaces including wood, skin, metals, and plastic. Yet, the underlying mechanisms remain poorly understood. Here, an investigation of the adhesive performance of mistletoe viscin is performed, demonstrating its hygroscopic nature and ability to self-heal following adhesive failure. It is identified that adhesion originates from a water-soluble adhesive component that can be extracted, isolated, and characterized independently. Lap shear mechanical testing indicates that the mistletoe adhesive extract (MAE) outperforms native viscin tissue, as well as gum arabic and arabinogalactan—common plant-based adhesives. Furthermore, humidity uptake experiments reveal that MAE can reversibly absorb nearly 100% of its mass in water from the atmosphere. In-depth spectroscopic and mass spectrometry investigations reveal a composition consisting primarily of an atypical arabinogalactan, with additional sugar alcohols. Finally, several proof-of-concept applications are demonstrated using MAE for hygro-responsive reversible adhesion between various surfaces including skin, plastic, PDMS, and paper, revealing that MAE holds potential as a biorenewable and reusable adhesive for applications in cosmetics, packaging, and potentially, tissue engineering.

1. Introduction

In recent decades, materials scientists have increasingly aimed to apply design principles extracted from biological materials to improve the performance and sustainability of man-made materials. As cellulose is the most widely abundant polymer in the natural world, plant-derived and plant-inspired materials aid researchers as blueprints for the design of green materials in wide-ranging fields with an overarching goal of minimizing human dependence on petroleum-based polymers.[1–5] In the realm of adhesives, crude oil-derivatives such as polyurethane (PU) and polyvinyl acetate (PVA) are widely used, especially as wood glues.[6,7] Though efforts are expanding to produce these adhesives from alternative source materials,[8] nature provides numerous relevant model systems which use environmentally benign building blocks to achieve excellent adhesion properties including well-studied systems such as gecko toe pads and the mussel byssus.[9,10] Recently, mistletoe has emerged as a

S. D. George, E. Andraos, T. Priemel, M. J. Harrington
Department of Chemistry
McGill University
801 Sherbrooke Street West, Montreal, Quebec H3A 0B8, Canada
E-mail: matt.harrington@mcgill.ca

N. Horbelt
Department of Biomaterials
Max-Planck Institute of Colloids and Interfaces
Science Park Potsdam-Golm, 14424 Potsdam, Germany

G. Keiser, A. Kumar, C. Heiss, P. Azadi
Complex Carbohydrate Research Center
University of Georgia
Athens, GA 30602, USA

N. Gierlinger
Department of Nanobiosciences
University of Natural Resources and Life Sciences Vienna (BOKU)
Vienna 1190, Austria

The ORCID identification number(s) for the author(s) of this article can be found under https://doi.org/10.1002/adfm.202307955

DOI: 10.1002/adfm.202307955

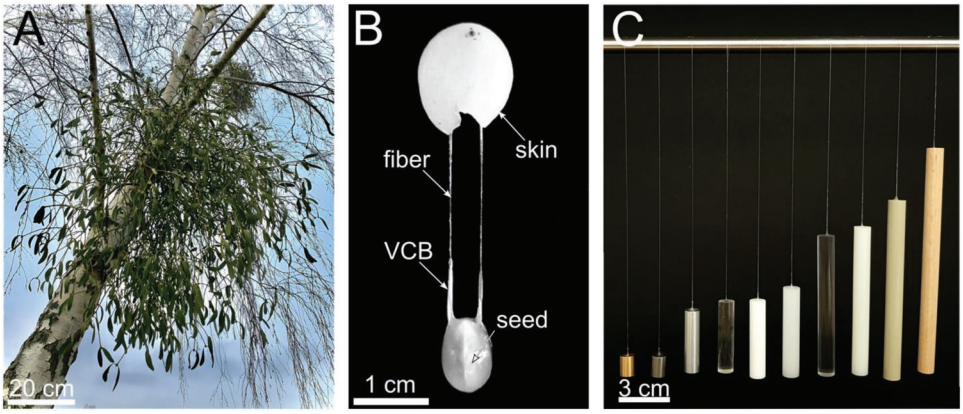

Figure 1. Mistletoe viscin adhesive capacity. A) View of a mistletoe (*V. album ssp. album*) plant with berries growing on a deciduous host. B) Extraction of the seed from a mistletoe berry results in fiber formation extending from the viscin cell bundles (VCBs). C) Viscin tissue from mistletoe demonstrates adhesion to a range of synthetic and natural materials, from left to right: brass, stainless steel, aluminum, quartz glass, polytetrafluoroethylene (PTFE), high density polyethylene (HDPE), polycarbonate (PC), polyamide (PA), polypropylene (PP), and beech wood. Each cylinder is 1 cm in diameter and 10 g in mass. The image in panel (B) is used from reference 11 under a CC BY 4.0 license (https://creativecommons.org/licenses/by/4.0/).

new role model for the development of biorenewable adhesive technologies.[11]

Recognizable by its pale white berries which grow in winter (**Figure 1**A,B), the European mistletoe (*Viscum album* L. *ssp. album*) is an aerial hemiparasitic plant species which has evolved to grow on the branches of host trees. This requires that its seeds can stick to a host branch for successful germination (often after passing through the digestive tract of a bird).[12–14] To achieve this, the seeds are surrounded by a mucilaginous sticky tissue known as viscin, with two horn-like appendages attached at the base of the seed known as the viscin cell bundles (VCBs), which contain cells in which tightly coiled cellulose microfibrils are wrapped perpendicular to the long cell axis (Figure 1B).[15] Previous studies revealed that the VCB is highly mechanoresponsive and can be drawn with minimal tensile forces into stiff and strong adhesive fibers that can extend from just ≈5 mm up to several meters in length, increasing the likelihood of catching on a tree branch (Figure 1B).[12,16,17]

More recent investigations reveal that viscin's adhesive capabilities extend beyond just wood and bark, seemingly indiscriminate in terms of the surface chemistry to which the tissue sticks, whether hydrophilic, hydrophobic, synthetic, or even biological materials (e.g., skin and cartilage) (Figure 1C).[11] Notably, the mechanoresponsive and adhesive properties of viscin can be reversibly modulated in a controlled way with humidity—dried viscin tissue and fibers are rigid and non-adhesive, but they can rapidly take up humidity from the atmosphere rendering them sticky and pliable. In this hydrated state, viscin will adhere to nearly any surface and can be mechanically reshaped or fused together with other viscin fibers. However, this hygroscopic adhesion and processing mechanism is still poorly understood.[11,16] Hygro-responsive behavior in plant systems has been primarily studied in context of work-intensive actuated bending, twisting, or ejection motions, and shown to involve uptake of water by hemicellulosic polymers between stiff cellulose fibers in the cells that make up the materials.[18–22] Similarly, in mistletoe, humidity uptake was shown to involve the swelling of a non-cellulosic matrix between cellulose microfibrils.[16]

Despite its importance, the swellable, adhesive matrix from mistletoe remains uncharacterized in terms of its performance and chemical composition. Yet, a physical and chemical understanding of the underlying mechanisms is essential to transfer design principles for application in green adhesion technologies. Here, we performed a mechanical and spectroscopic investigation of mistletoe adhesion to elucidate key structure–function relationships. Our findings indicate that mistletoe viscin employs a chemical adhesion mechanism, with the capacity to self-heal due to reversible hygroscopic activation. Moreover, we isolate a water-soluble biomolecular extract that is responsible for the adhesive properties of mistletoe berries. Mechanical, spectroscopic and mass spectrometric analysis reveals that this component is polysaccharidic in nature, but distinctive functionally and compositionally from other common plant-based adhesives. These results suggest that the mistletoe adhesive extract (MAE) could provide a compelling sustainable alternative for petroleum-based adhesives with advanced functionalities relevant in numerous industries.

2. Results and Discussion

2.1. Multi-Material Adhesion

It was previously shown that mistletoe viscin adheres to a variety of surface chemistries both natural and synthetic (Figure 1C).[11] However, quantification of the adhesive strength of mistletoe viscin across different materials was not examined. A standard single-lap shear test was employed using small strips of wood (birch), polystyrene plastic (PS), aluminum, and copper adhered with viscin tissue in a square geometry (**Figure 2**A) under humidity conditions between 30 and 32% relative humidity (RH). Of these four surface chemistries, wooden samples demonstrated the highest shear breaking strength, with a mean value of 1.17 ± 0.28 MPa (Figure 2B). The copper samples demonstrated an average breaking strength around 0.39 ± 0.18 MPa, while aluminum and PS around 0.25 ± 0.09 and 0.25 ± 0.18 MPa, respectively. Statistical analysis revealed that the wooden samples were

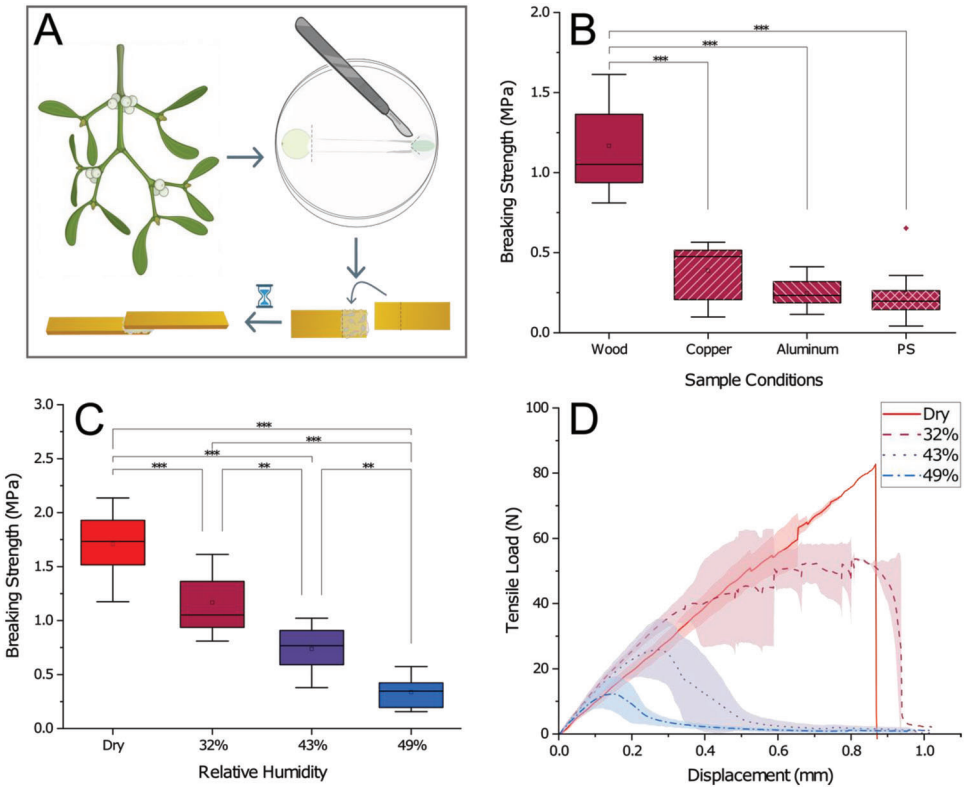

Figure 2. Surface and humidity-dependent adhesive strength of mistletoe viscin. A) Sample preparation of lap shear tensile testing. Two strips of substrate material are held together by adhesive mistletoe viscin over a square-shaped overlap area. Created with BioRender.com. B) Comparison of mistletoe viscin lap shear sample breaking strengths across four different material surfaces. Samples tested between 30% and 32% RH. For (B) and (C), $^{**}p \leq 0.01$, $^{***}p \leq 0.001$ using one-way ANOVA with Tukey-Kramer HSD post-hoc test. C) Wooden samples' breaking strengths at different testing humidity conditions. D) Using the same data sets from (C), the measured force data were used to calculate average load values at each displacement position, shown as the plotted lines with the standard deviation for each displacement value represented as respective shadows behind the plots (all plots shown in Figure S1, Supporting Information). The colors for each RH value from (C) correspond here and throughout the manuscript according to testing conditions of all displayed datasets. N is between 6 and 10 for all mechanical datasets.

significantly different than the three other materials in terms of breaking strength, while the aluminum, copper, and PS samples were not significantly different from one another. Because *V. album* has evolved to germinate onto tree branches, the surface chemistry of wood or bark is likely the optimal surface for viscin, and it is reasonable that wood shows a higher adhesive strength.

2.2. Humidity Dependent Mistletoe Adhesion

Previous lap shear testing at low and high humidity conditions suggested viscin's hygro-responsive properties influence adhesive strength; however, this was not extensively characterized.[11] To further explore the impact of moisture-uptake on viscin adhesive strength, wooden single-lap shear samples were tested after equilibration at four different humidity conditions, ranging from dry (<20% RH) to 49% RH (Figure 2C, Figure S1, Supporting Information). Higher breaking strengths were measured at the driest conditions with a mean of 1.71 ± 0.31 MPa, and the adhesive strength decreased as humidity increased, with samples averaging 0.34 ± 0.14 MPa at 49% RH (Figure 2C). Examination of the force-displacement curves reveals that the observed failure mode is also humidity dependent. Samples measured under dry conditions exhibit brittle-like failure at higher forces without undergoing an obvious yield event (Figure 2D, Figure S1, Supporting Information). In contrast, the force-displacement curves measured at 43% and 49% RH conditions show a clear yield point at low force, followed by extended ductile deformation before failure. The dataset at 32% RH reveals a mixture of the two failure modes, which is not surprising since previous studies showed that mistletoe viscin fibers undergo a significant decrease in tensile stiffness in the range of 30–45% RH, due to a rapid increase in moisture-uptake within this range, maxing out at 34% moisture content at 95% RH.[16] Notably, under both high and low humidity conditions, SEM imaging of fracture surfaces provides evidence of crazing as suggested by the presence of microvoids bridged by small fibrils (Figure S2, Supporting Information).[23] This may, therefore, provide a toughening mechanism in both dry and humid samples that enhances the strength of the adhesive layer through load deflection despite material fatigue. Finally, the fact that successful adhesion requires application of viscin in the wet state with drying and applied load required to effectively cure the glue indicates that viscin would not be considered a pressure-sensitive adhesive.

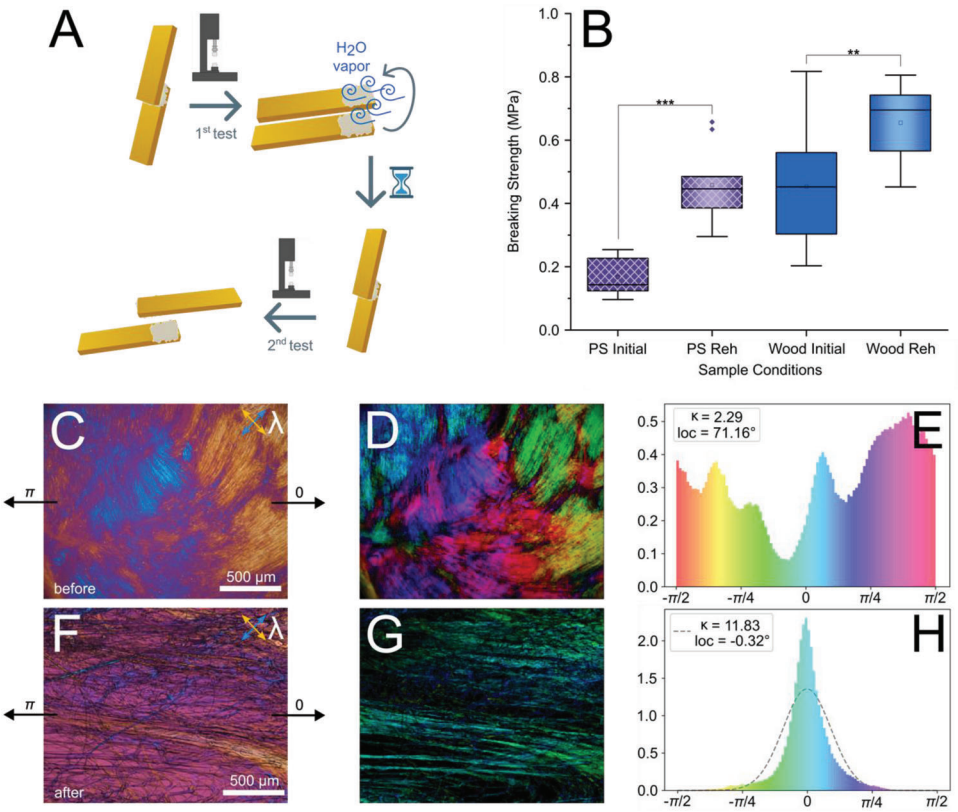

Figure 3. Self-healing adhesion with mistletoe viscin. A) Schematic of re-adhesion process: after initial testing, samples were held over water vapor and subsequently pressed back together to cure before a second round of lap shear testing. Created with BioRender.com. B) Comparison of initial and rehydrated ("Reh") breaking strengths for two sample sets. The polystyrene (PS) sample set was tested at 41–42% RH, the wooden sample set at 47% RH. $^{**}p \leq 0.01$ and $^{***}p \leq 0.001$ using one-way ANOVA with Tukey-Kramer HSD post-hoc test. N is between 9 and 12 for all mechanical datasets presented. C) PLM image, with full-wave retardance plate, of a single lap shear sample prepared between two glass slides as shown before testing. D,E) The orientation of CMFs within the viscin tissue's cells, with reference to the horizontal axis of tensile load defined in (C). E,H) A von Mises distribution describes the angular distribution of cellulose fibril orientations. Kappa (κ) is a measure of concentration or uniformity of the distribution, and "loc" refers to the angle of local orientation for the entire area of analysis. F) PLM image of the same sample as in (C) after testing, set in the same orientation. G,H) The orientation of cellulose fibers formed along the load axis upon lap shear testing. Images and data analysis in panels (C)–(H) come from a single sample measured before and after mechanical lap shear testing. However, averaged data from $N = 5$ samples is found in the text in Section 2.3.

2.3. Hygroscopic Self-Healing and Fiber-Reinforced Adhesion

Based on the hygroresponsive fiber welding functionality of viscin tissue demonstrated previously,[11] we explored the possibility that failed adhesive surfaces could be self-healed. Adapting previous protocols,[11] we rehydrated fractured lap shear test samples, using water vapor, re-adhered the two surfaces, and retested their lap shear adhesive strength (**Figure 3**A). Our results indicate that not only was healing possible using this method, but that healed samples showed a statistically significant increase in breaking strength for both PS and wooden samples (Figure 3B).

To further investigate the mechanism of increased adhesive strength in healed samples, we acquired a series of polarized light microscopy (PLM) images of lap shear samples adhered between glass slides over a range of polarization angles before and after mechanical testing (Figure 3C–H). Preferred angular orientation of birefringent cellulose microfibrils was plotted as a von Mises distribution for each individual sample[24] (Figure 3E,H) providing a kappa value (κ), which is a measure of concentration or uniformity in the angular distribution, where a higher kappa value indicates a more highly oriented sample. The von Mises model also provides the angle of preferential orientation (loc), considering the entire image field of view. Freshly prepared lap shear samples showed low preferential alignment ($\kappa = 2.7 \pm 0.7$), with a cellulose orientation distribution across all possible angles (Figure 3E), as clearly demonstrated in the recolorized PLM micrograph showing corresponding angular orientation (Figure 3D). Before testing, angular distribution is dependent on the placement of the viscin tissue between the two surfaces, resulting in no preferred angle of cellulose orientation in a population of samples as indicated by an arbitrary mean orientation angle across samples and an enormous standard deviation (loc = $-15.0° \pm 74.8°$). Note that these are averaged values for all analyzed samples ($N = 5$).

In contrast, PLM analysis of the same lap shear samples after mechanical testing reveals cellulose fibers within the adhesive layer of all samples are preferentially aligned along the axis of mechanical load (Figure 3F,G). The von Mises distribution analysis averaged from $N = 5$ samples shows a stark increase in preferred orientation ($\kappa = 11.8 \pm 2.2$) with a tight angular distribution in

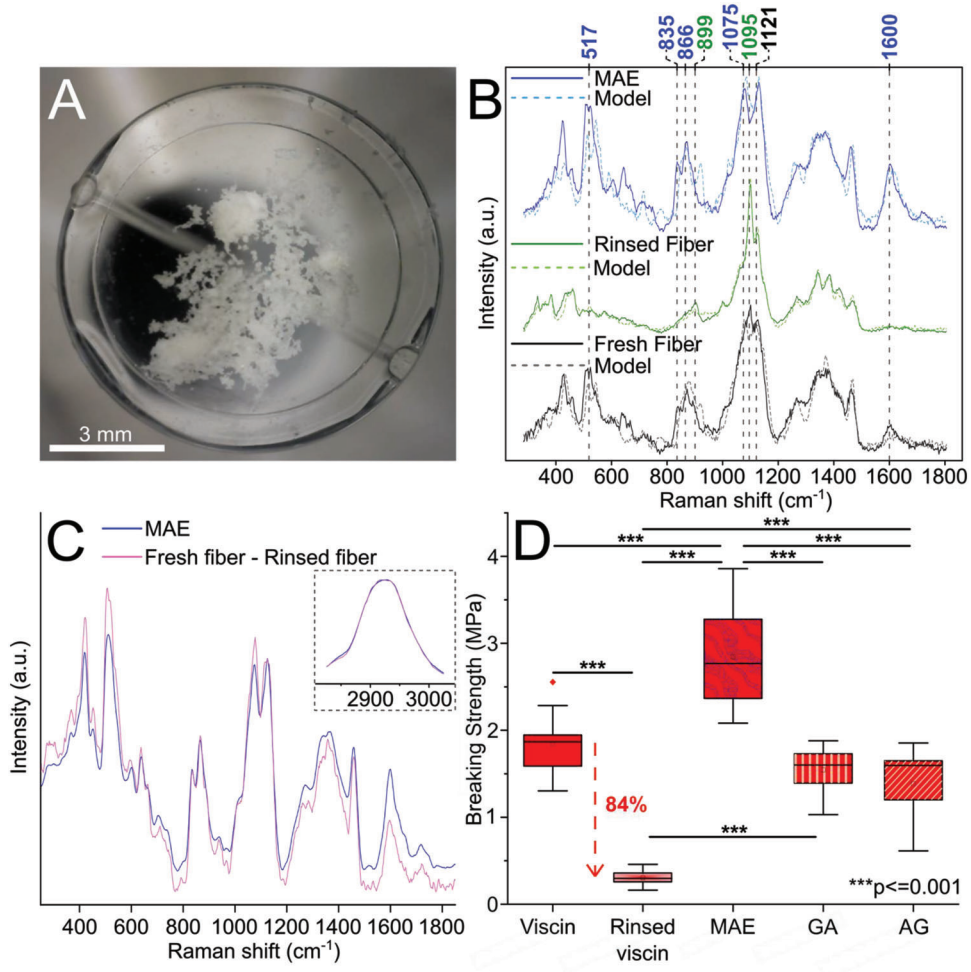

Figure 4. A water-extractable component provides adhesive functionality to mistletoe. A) Image of the freeze-dried MAE powder at 0% RH. B) Confocal Raman spectra for a native viscin fiber, a fiber formed from water-rinsed viscin, and MAE powder. A reference database for plant polysaccharides was used to fit predictive compositional models to each dataset shown as dotted lines. C) The Raman spectrum of the MAE powder is overlaid with a difference spectrum resulting from the subtraction of averaged water-rinsed fiber spectra multiplied by a prefactor of 0.2 from the averaged native fiber spectra. Spectra were normalized to the C–H band (see inset). D) Lap shear samples comparing native viscin, rinsed viscin, and MAE, as well as standards of gum arabic (GA) and arabinogalactan (AG). All sample sets were tested on wood between 20% and 23% RH and N was between 8 and 10 for all datasets. Samples are marked statistically different from one another at $***p \leq 0.001$ using Tukey-Kramer HSD post-hoc test after one-way ANOVA, except the native viscin, gum arabic, and arabinogalactan sets which are not statistically different.

close agreement with the horizontal load axis (loc = 0.4° ± 3.9°) (Figure 3H). These results suggest that mechanical forces during the first loading cause alignment of cellulose microfibrils in the viscin tissue, consistent with previous investigations of viscin fiber drawing.[16] When aligned within the adhesive layer, these fibers will mechanically reinforce the adhesive such that upon rehydration and curing, the strength of the healed adhesive along the axis of load is increased (Figure 3B).

2.4. Water-Soluble Viscin Extract Is the Principal Adhesive Component

Our mechanical investigation suggests a mechanism of adhesion and self-healing that is dependent on specific chemical interactions given the different adhesive strengths on different material surfaces. Thus, we sought to further characterize its molecular basis. Azuma and colleagues previously observed that viscin tissue from *V. album* loses its stickiness when rinsed in water;[15] however, the adhesive properties of washed viscin (which they called viscan) were not characterized mechanically. To confirm their observation and to quantify the effect on adhesive strength, viscin tissue was rinsed with MilliQ (MQ) water and tested in lap shear geometry resulting in a significant loss of adhesive strength by over 80% on wood surfaces and over 70% on PS surfaces. (**Figure 4**D, Figure S3, Supporting Information). Similarly, we also observed that self-healing of viscin (Figure 3B) was less effective when fractured sample surfaces were rinsed prior to re-adhesion (Figure S4, Supporting Information). These observations indicate that there is a functional water-soluble adhesive component or components present in the native tissue, and suggest that specific aspects of the chemical structure of this

component contribute significantly to viscin tissue adhesion and healing (i.e., adhesion is not simply the result of mechanical interlocking).

Because the adhesive component was solubilized into MQ water, it was possible to isolate it by lyophilization of the liquid used to rinse the viscin, resulting in a white powder, which we call mistletoe adhesive extract (MAE) (Figure 4A). Raman spectroscopic analysis of MAE shows broad carbohydrate bands similar to native viscin, while the rinsed fiber spectrum has fewer, yet sharper bands (Figure 4B). Indeed, spectral subtraction of native minus rinsed sample spectra is nearly identical to the spectrum from MAE (Figure 4C), confirming that MAE is chemically distinct from the remaining viscin material after washing, which was previously characterized by Azuma and colleagues.[15] Humidity uptake experiments using dynamic vapor sorption (DVS) demonstrate that MAE is capable of reversibly taking up 99% of its weight in water, which is approximately double that of control standards gum arabic (GA) and arabinogalactan (AG) (Figure S5, Supporting Information) and as previously shown, is nearly triple that of the native viscin tissue,[16] which contains many other components including cellulose microfibrils. Notably, MAE only shows significant moisture uptake after reaching ≈30–40% RH, which is consistent with our adhesion studies and previous studies of viscin fiber stiffness.[16] Together, these data establish MAE as a prime candidate for the hygro-responsive adhesive component in viscin.

To determine if MAE could be the principal adhesive component in mistletoe viscin, we performed a functional adhesion comparison with standards of gum arabic and arabinogalactan, employing lap shear tests on wooden samples at low RH conditions (20–23% RH) (Figure 4D). Gum arabic has a long history as a polysaccharide extract from the *Acacia senegal* tree that has been used by humans for over 5000 years in various adhesive applications including pigmentation in paints or more recently in cosmetics and lithographics,[25] while recent studies reveal that arabinogalactan's highly branched structure provides intermolecular forces demonstrated as beneficial for adhesive applications.[26] To employ MAE as an adhesive, it was first necessary to activate the freeze-dried residue by locally elevating the humidity briefly using a nebulizer (although adding very small relative volumes of water has a similar effect). Afterward, the hygro-activated MAE could be pressed between the surfaces and dried. The adhesive strengths of gum arabic and arabinogalactan prepared in the same way were comparable to the native viscin tissue, averaging between 1.4 and 1.8 MPa, while MAE exhibited a significantly higher mean strength of 2.85 ± 0.61 MPa. These results support the hypothesis that MAE provides adhesive functionality to viscin and indicate that MAE can be used independently as a highly effective bio-sourced adhesive.

2.5. Compositional Analysis of Mistletoe Adhesive Extract

Previous compositional analysis of mistletoe viscin from *V. album* was focused specifically on rinsed viscin (a.k.a. viscan),[15] but this was presumably depleted of MAE. Here, we investigated the chemical composition of MAE, as well as native and washed viscin fibers, by fitting acquired Raman spectra with a database of plant component spectra using an orthogonal matching pursuit algorithm (Figure 4B,C, details in Figure S6, Supporting Information). Washed viscin yielded the best fit—the strong sharp bands coincide with the cellulose spectrum with bands at 1122 and 1095 cm^{-1}, while the model could fit arabinan and a pectinic galactan residues as minor components (Figure S6C, Supporting Information), consistent with previous compositional analysis.[15] A reasonable fit of native fiber spectra could be reconstructed based on cellulose spectra and arabinogalactan, as well as 1,3-glucan, and glucose (Figure S6D, Supporting Information). Notably, however, the model for MAE yielded the weakest fit, suggesting arabinogalactan as a primary component but with significant differences that could not be matched convincingly to the database (Figure S6A, Supporting Information). This suggests either that MAE contains additional components that are missing from the database or that it has a fundamentally different structure than the database arabinogalactan (from larch wood). Indeed, Raman spectra from carbohydrates can vary significantly as they change from monosaccharides to disaccharides to polysaccharides and depend on the sugar units in backbone linkages and side chains.[27]

To gain further insights into the chemical structure of MAE, we performed glycosyl analysis by gas chromatography-mass spectrometry (GC-MS) and one- and two-dimensional NMR spectroscopy (**Figure 5**). Consistent with Raman, the results indicate that the unknown polysaccharide is an atypical arabinogalactan. Initial compositional analysis showed the most abundant monosaccharide detected in the native sample to be glucose present as the free monosaccharide, but after dialysis, arabinose (Ara) and galactose (Gal) composed 51.6% and 36.4%, respectively, of MAE by mole percentage. Linkage analysis by methylation and gas chromatography after sample dialysis revealed the most abundant residues as terminal and 5-linked Ara*f*, as well as 3,6-linked and 6-linked Gal*p* (Table S1, Supporting Information).

2D NMR analysis of the dialyzed sample confirmed these findings, indicating the substantial presence of α-arabinofuranose and β-galactopyranose, with the β-Gal*p* residues showing characteristic anomeric ^{1}H shifts around 4.5 ppm and the cluster of α-Ara*f* residues with varying linkages toward 5.1 ppm (Figure 5B–D and Table S2, Supporting Information). Additionally, the analysis of α-glycosylation shifts and degree of substitution for Ara*f* and Gal*p* residues at each carbon on the sugar rings. ^{1}H-^{13}C HMBC analysis (Figure S7, Supporting Information) also indicated connections between separate residues, revealing direct bonding between these specific monosaccharides. Together with GC-MS, the NMR provided convincing support to the GC-MS results regarding the presence of various glycosidic linkages (Table S2, Supporting Information with details regarding analysis). These results indicate a 1,6-linked β-galactan chain abundant with terminal and 5-linked α-Ara*f* residues attached to O-3 of 2 out of 3 Gal*p* backbone residues (Polysaccharide II, Figure 5D). Though atypical for other so-called arabino-3,6-galactan structures,[28] these findings are in agreement with a previously published structure of an arabinogalactan identified in *V. album*.[29] However in their study, the authors used an entire-berry extraction and did not identify any adhesive functionality. The arabinogalactan found in MAE falls into the category of less common AGs with a 1,6-linked β-galactan main chain very recently designated as "type II related AG."[30] Research on other plants containing type II related AGs has been almost exclusively focused on food and medicinal

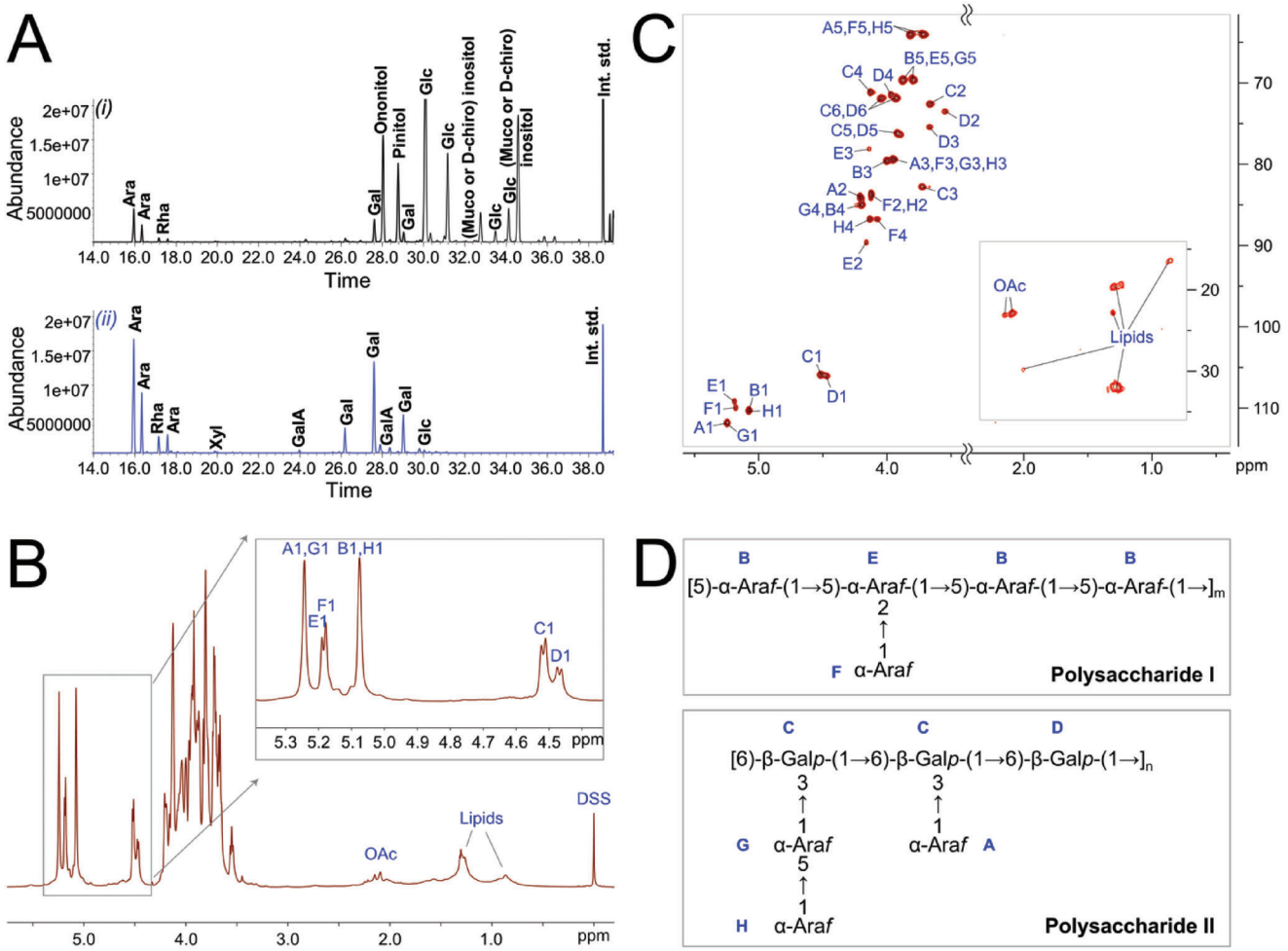

Figure 5. Glycosyl composition and NMR structural analysis of MAE. A) GC chromatograms of MAE powder. The native sample (*i*) consisted of high quantities of glucose and isomers of inositol and inositol methyl esters, ononitol and pinitol. These were recognized using the National Institute of Standards and Technology (NIST) database but could not be unambiguously identified due to lack of authentic standards. To remove glucose and the inositol isomers, dialysis was performed. The dialyzed sample (*ii*) consisted of arabinose and galactose, providing evidence for arabinogalactan side chains. B) ^{1}H NMR and C) ^{1}H-^{13}C-HSQC NMR spectra of *V. album*, acquired in D_2O on a 600 MHz Bruker spectrometer equipped with a 5-mm cryoprobe, showing representative labels corresponding to anomeric protons of identified sugar residues including α-arabinose and β-galactose. D) Proposed structures of the polysaccharide side chains based on 1D and 2D NMR analysis.

applications of the polysaccharides and related proteins and aromatics for antioxidant or immunoactivation purposes.[31,32]

In addition to arabinogalactan, these results suggest the presence of other components. An arabinan of 1,5-linked α-Ara*f* with occasional 2-linked α-Ara*f* side chains is evident, but it is presently unclear whether this arabinan is present as a bound species with the arabinogalactan or as a separate polysaccharide (Polysaccharide I). The prior study by Wagner and Jordan proposed that Polysaccharides I and II were covalently linked to a rhamnogalacturonan-I (RG-I) backbone.[29] As we also detected both 2,4-linked rhamnose (Rha) and 4-linked galacturonic acid (GalA) in the glycosyl linkage analysis (Table S1, Supporting Information), this could correspond to this pectinic sugar. However, the abundance of Rha and GalA residues in our sample was so low, we could not pick them up using NMR. Finally, small sugar alcohols such as inositol were identified during compositional analysis, although these were mainly removed along with free glucose via dialysis. Further analysis is required to identify the specific branching and covalent bonding present in the MAE residue and characterize each component's functional role within the system.

2.6. Proof-of-Concept Applications of Mistletoe Adhesive Extract

Based on the demonstrated adhesive capacity of viscin tissue,[11] we explored the potential for using MAE as an effective and reversible adhesive for industrially and biomedically relevant applications (**Figure 6**). As a first example, we utilized MAE to seal a paper envelope, demonstrating the ability to reversibly seal and open the envelope over ten times using cycles of water vapor application and drying. Attempting to open the envelope without application of humidity resulted in ripping of the paper (similar to a standard envelope) indicating the high strength of the

Figure 6. Practical applications of mistletoe adhesive extract. MAE can act as an effective glue upon rehydration with water vapor or mixing with a small quantity of water. The glue was used to reversibly adhere paper to paper (envelope), paper to skin (googly eye), plastic to skin (decorative gem), and PDMS to skin (microfluidic device).

adhesion. Toward cosmetic and decorative applications, we demonstrated that MAE could be used to reversibly adhere objects with both paper and plastic backings onto human skin (Figure 6). Finally, a portion of a microfluidic device cast in polydimethylsiloxane (PDMS) was adhered to skin (Figure 6) to simulate cutting edge epidermal devices currently used to measure a variety of clinical diagnostics such as sweat rate or electrical activity produced by the heart and brain.[33,34] These objects remained adhered to the skin many hours, up to 24 h in one case, but they were all simply and easily removed when desirable by application of high humidity (>90%) or rinsing with running water. While we did not test the effect of profuse sweating on adhesion, normal everyday activities and skin's localized humidity did not result in loss of adhesion. These examples underline the potential of plant-sourced MAE for a range of different applications normally handled by petroleum-based glues.

3. Conclusion

Our findings indicate that MAE is a highly promising candidate for a biorenewable plant-sourced adhesive with many advantages over current comparable extracts (e.g., gum arabic)—including higher adhesive strength, increased hygroresponsivity, and reversibility. Considering that gum arabic has been used for nearly 5000 years in various applications,[35] the potential applications of MAE are numerous. Moreover, the strong and reversible hygroscopic adhesive response of MAE endows it with clearly demonstrated reusability and self-healing capacity which will be useful in many areas including cosmetics and packaging in the paper industry, as well as biomedical applications.

Although still incomplete, elucidating the chemical composition of MAE provides the first steps toward understanding the chemical mechanisms of reversible adhesion and humidity uptake, and thus, the first steps toward mimicking this behavior. For example, the discovery of catechol-based adhesion in marine mussels has propagated enormous breakthroughs in development of underwater adhesives,[36] while the fundamental understanding of gecko adhesion has resulted in commercialized gecko-inspired reversible tapes.[37] Similarly, we anticipate that a deeper understanding of the adhesive chemistry of mistletoe will spark analogous breakthroughs in reversible adhesive technologies. Indeed, through systematic and thorough characterization of the various chemical components in MAE, their structure, and their function, it should be possible to directly link the adhesive prowess of MAE to specific chemical features. Nonetheless, even without a full mechanistic understanding, we demonstrate that MAE is an easily extracted adhesive material that can be directly used for relevant applications. Considering that the European mistletoe is a highly abundant parasitic plant that colonizes host trees across Europe, and that a single plant contains thousands of berries each of which can generate ≈10 mg of MAE residue, this is a biorenewable technology that is ripe for the picking.

4. Experimental Section

For full experimental details, see the Supporting Information.

Samples: Mature berries from European mistletoe (*V. album ssp. album*) were collected and flash frozen in liquid nitrogen for long-term storage at −20 °C. For lap shear test surfaces, birch wood sticks (Couche-Tard), polystyrene (Fischer Scientific), flat 21 gauge bare copper craft wire (Artistic Wire), flat 18 gauge aluminum wire (PandaHall), and glass microscopy slides (VWR) were used. For comparative studies two polysaccharide standards were used: Gum arabic from acacia tree (Sigma) and (+)-Arabinogalactan from Larch Wood (TCI America).

Lap Shear Mechanical Testing: Berries were thawed at room temperature, and the viscin tissue was isolated after seed extraction using a tweezer and scalpel. The viscin was sandwiched between the test surfaces and pressed together using tweezers for ≈15–20 s to ensure full contact and combat sample sliding. The overlap area was measured using Fiji in order to calculate the shear breaking strength. Samples were stored under controlled RH for a minimum of 4 h prior to testing. A typical dry mass of the adhesive layer of a sample was measured to be about 4.8 mg (mean of $N = 10$ samples equilibrated on wood at 23% RH). Lap shear mechanical testing was performed using an Instron Mini 44 Series Testing System (Artisan Technology Group) with an extension rate of 1.27 mm min^{-1}. For self-healing experiments, the tested samples were rehydrated for 10 min over MilliQ water vapor from a portable compressor nebulizer (100 for), then gently pressed together, cured, and tested again according to the above procedure.

Raman Spectroscopy: Raman spectroscopy was performed using a confocal Raman microscope (Alpha 300R, WITec) with a 532-nm green laser (power = 5 or 10 mW). Samples were focused using a 50× or 100× objective (Zeiss, numerical aperture [NA] = 0.8, 0.9, respectively). Spectra were collected with a thermoelectrically cooled CCD detector behind a 600-g mm^{-1} grating. For each single spectrum, a 5 s integration time was applied for 20 accumulations. A database of plant Raman spectra was used to create fits for predictive compositional models of the acquired raw spectra. The models were a combination of selected component reference spectra, chosen by an orthogonal matching pursuit algorithm to minimize the residual error after adding spectrum by spectrum. All models' residuals and spectral component plots are found in Figure S7 (Supporting Information). The difference spectrum in Figure 4C was produced as a result of subtracting averaged fresh fiber spectra minus the averaged rinsed fiber

multiplied by a prefactor of 0.2. This prefactor was chosen as the result of an iterative process to produce a difference spectrum without negative peaks.

Quantitative Polarized Light Microscopy (QPLM): Lap shear samples prepared on glass slides were imaged with QPLM before and after tensile testing (18–20% RH, $N = 5$) using an imaging system similar to the one developed by Glazer, Lewis, and Kaminsky.[38] A cross-polarized light microscope (Axio Scope.A1, Zeiss) with a 6-megapixel CCD camera (Axiocam 506 color, Zeiss) was further equipped with a 532 nm premium bandpass filter (FWHM = 10 nm) and a zero-order quarter-wave plate (532 nm) (Thorlabs). The quarter-wave plate was placed after the linear polarizer at a 45° angle toward the polarization axis to achieve circularly polarized monochromatic light for sample illumination. Using a rotating analyzer, the samples were imaged every 10° for a full 360° rotation. The intensity of pixels in the images at different polarizations were analyzed using our own Python script (Code S1, Supporting Information), which provides as an output the local orientation of the cellulose fibers as a false color image and a histogram (details reported in Supporting Information). The histogram is subsequently fitted to a von Mises distribution resulting in an average orientation (loc) and a concentration factor κ, which represents the overall alignment of the molecules in the sample.

MAE Extraction: VCBs were isolated from several berries and thoroughly rinsed in MQ water (1.0 mL) in a microcentrifuge tube for 30 s using an analog vortex mixer (VWR) on the highest setting. During mixing, the tube was tilted at various angles to facilitate turbulent mixing. The solid VCB was removed and discarded, and the tube was centrifuged to pellet any smaller solid particles. The supernatant was collected and flash frozen in liquid nitrogen followed by lyophilization to yield isolated MAE. This process can also be applied to the mucilage around *V. album ssp. album* seeds to increase yield, though centrifugation is essential to isolate only water-soluble components.

Dynamic Vapor Sorption: Experiments were conducted on a Surface Measurement Systems DVS Resolution instrument using a full-cycle sorption-desorption method, ramping from 0% to 95% RH incrementally, followed by desorption to 0% RH using a stream of N_2. At each RH% step, the material was allowed to equilibrate to a mass change (dm/dt) 0.002% for a period between 10 and 240 min. Additionally, samples were recorded by an in situ digital camera at every second RH% increment step. The temperature was kept constant at 25 °C for all polysaccharide samples.

GC-MS: Glycosyl composition analysis was performed by combined gas chromatography-mass spectrometry (GC-MS) of the per-*O*-trimethylsilyl (TMS) derivatives of the monosaccharide methyl glycosides produced from the MAE powder after acidic methanolysis and using *myo*-inositol as an internal standard. The analysis was performed as described previously by Santander et al.[39] with details reported in the Supporting Information.

NMR Spectroscopy: For all NMR experiments, dialyzed sample weighing ≈5 mg was dissolved in 1.0 mL D_2O (99.9% D) and lyophilized. Next, the sample was dissolved in 0.350 mL of D_2O and transferred to a 5-mm Shigemi NMR tube. All NMR data were acquired at 70 °C on a Bruker Avance III spectrometer (^{1}H, 600.06 MHz) equipped with a cryoprobe using standard pulse sequences. ^{1}H spectra, as well as 2D COSY, NOESY, TOCSY, HMBC, and HSQC spectra were all performed, with experimental details reported in the Supporting Information. The spectra were processed and analyzed with MestreNova (version 14.0.1-23559).

Statistical Analysis: All mechanical testing data were processed for statistical analysis using OriginPro 2021 software. These data underwent analysis using one-way analysis of variance (ANOVA) with Tukey-Kramer HSD post-hoc test, chosen to evaluate all comparison between sample group means amidst uneven sample sizes between groups. A significance level of $\alpha = 0.05$ was used in all analyses, and corresponding post-hoc result labels between groups were defined in the figure captions, ranging from $^{**}p \leq 0.01$ to $^{***}p \leq 0.001$. Data were presented using (mean ± SD) format. The sample sizes for lap shear mechanical testing groups ranged from $N = 6$–12 samples, specified in the Figure captions and corresponding text.

For QPLM analysis, $N = 5$ samples adhered on glass were used, and the von Mises distribution analysis was carried out using a Python code written by the authors and executed through the open-source development environment Spyder. The analysis code is available as Code S1 (Supporting Information). Further details regarding QPLM analysis are available in the Supporting Information.

Supporting Information

Supporting Information is available from the Wiley Online Library or from the author.

Acknowledgements

The authors thank T. van de Ven for access to the mechanical tester, H. Titi of the McGill Chemistry Characterization (MC^2) Facility for assistance with DVS data collection, and M. Cerruti and R. Allgayer for assistance in SEM imaging. S.D.G. acknowledges support from the FRQNT Québec Merit Award (B2X 317483). M.J.H. acknowledges funding through the Wares Scientific Innovation Prospector's Fund and a Canada Research Chair Award (CRC Tier 2 950-231953). This study was supported in part by GlycoMIP, a National Science Foundation Materials Innovation Platform funded through Cooperative Agreement DMR-1933525 and the U.S. Department of Energy, Office of Science, Basic Energy Sciences, Chemical Sciences, Geosciences and Biosciences Division, under award number DE-SC0015662.

Conflict of Interest

The authors declare no conflict of interest.

Data Availability Statement

The data that support the findings of this study are available in the supplementary material of this article.

Keywords

adhesion, arabinogalactan, bio-inspired materials, cellulose, fiber-reinforced, mistletoe viscin, self-healing

Received: July 11, 2023
Revised: August 28, 2023
Published online: October 22, 2023

[1] C. Wenig, J. W. C. Dunlop, J. Hehemeyer-Cürten, F. J. Reppe, N. Horbelt, K. Krauthausen, P. Fratzl, M. Eder, *Philos. Trans. R. Soc., A* **2021**, *379*, 20200345.
[2] S. H. Imam, S. H. Gordon, L. Mao, L. Chen, *Polym. Degrad. Stab.* **2001**, *73*, 529.
[3] S. Pradhan, A. K. Brooks, V. K. Yadavalli, *Mater. Today Bio* **2020**, *7*, 100065.
[4] T. Sippach, H. Dahy, K. Uhlig, B. Grisin, S. Carosella, P. Middendorf, *Polymers* **2020**, *12*, 3048.
[5] D. Gan, W. Xing, L. Jiang, J. Fang, C. Zhao, F. Ren, L. Fang, K. Wang, X. Lu, *Nat. Commun.* **2019**, *10*, 1487.
[6] M. D. Banea, L. F. M. da Silva, R. D. S. G. Campilho, *J. Adhes.* **2015**, *91*, 331.
[7] D. Aydemir, *BioResources* **2014**, *9*, 1179.
[8] K. P. Somani, S. S. Kansara, N. K. Patel, A. K. Rakshit, *Int. J. Adhes. Adhes.* **2003**, *23*, 269.

[9] M. Zhou, N. Pesika, H. Zeng, Y. Tian, J. Israelachvili, *Friction* **2013**, *1*, 114.
[10] M. J. Harrington, F. Jehle, T. Priemel, *Biotechnol. J.* **2018**, *13*, 1800133.
[11] N. Horbelt, P. Fratzl, M. J. Harrington, *PNAS Nexus* **2022**, *1*, 026.
[12] H. S. Heide-Jorgensen, *Parasitic Flowering Plants*, Brill Academic Pub, Leiden **2008**.
[13] J. Kuijt, *The Biology of Parasitic Flowering Plants*, University of California Press, Berkeley **1969**.
[14] M. D. Mylo, M. Hofmann, A. Delp, R. Scholz, F. Walther, T. Speck, O. Speck, *Front. Plant Sci.* **2021**, *12*, 715711.
[15] J. Azuma, N.-H. Kim, L. Heux, R. Vuong, H. Chanzy, *Cellulose* **2000**, *7*, 3.
[16] N. Horbelt, M. Eder, L. Bertinetti, P. Fratzl, M. J. Harrington, *Biomacromolecules* **2019**, *20*, 3094.
[17] D. Zuber, *Funct. Ecol. Plants* **2004**, *199*, 181.
[18] M. J. Harrington, K. Razghandi, F. Ditsch, L. Guiducci, M. Rueggeberg, J. W. C. Dunlop, P. Fratzl, C. Neinhuis, I. Burgert, *Nat. Commun.* **2011**, *2*, 337.
[19] S. Poppinga, A.-S. Böse, R. Seidel, L. Hesse, J. Leupold, S. Caliaro, T. Speck, *J. R. Soc., Interface* **2019**, *16*, 20190327.
[20] R. Elbaum, L. Zaltzman, I. Burgert, P. Fratzl, *Science* **2007**, *316*, 884.
[21] J. Ha, S. M. Choi, B. Shin, M. Lee, W. Jung, H.-Y. Kim, *Extreme Mech Lett* **2020**, *38*, 100746.
[22] C. Dawson, J. F. V. Vincent, A.-M. Rocca, *Nature* **1997**, *390*, 668.
[23] L. L. Berger, E. J. Kramer, *Macromolecules* **1987**, *20*, 1980.
[24] J. W. Y. Jor, P. M. F. Nielsen, M. P. Nash, P. J. Hunter, *Skin Res. Technol.* **2011**, *17*, 149.
[25] N. Prasad, N. Thombare, S. C. Sharma, S. Kumar, *Ind. Crops Prod.* **2022**, *187*, 115304.
[26] E. S. Wibowo, B.-D. Park, *Wood Sci. Technol.* **2022**, *56*, 1047.
[27] E. Wiercigroch, E. Szafraniec, K. Czamara, M. Z. Pacia, K. Majzner, K. Kochan, A. Kaczor, M. Baranska, K. Malek, *Spectrochim. Acta, Part A* **2017**, *185*, 317.
[28] A. E. Clarke, R. L. Anderson, B. A. Stone, *Phytochemistry* **1979**, *18*, 521.
[29] H. Wagner, E. Jordan, *Phytochemistry* **1988**, *27*, 2511.
[30] K. Ghosh, D. Takahashi, T. Kotake, *Carbohydr. Res.* **2023**, *529*, 108828.
[31] K. Ghosh, S. Ray, D. Ghosh, B. Ray, *Carbohydr. Polym.* **2015**, *117*, 370.
[32] S. Bahramzadeh, M. Tabarsa, S. You, K. Yelithao, V. Klochkov, R. Ilfat, *J. Funct. Foods* **2019**, *52*, 450.
[33] D.-H. Kim, N. Lu, R. Ma, Y.-S. Kim, R.-H. Kim, S. Wang, J. Wu, S. M. Won, H. Tao, A. Islam, K. J. Yu, T. Kim, R. Chowdhury, M. Ying, L. Xu, M. Li, H.-J. Chung, H. Keum, M. McCormick, P. Liu, Y.-W. Zhang, F. G. Omenetto, Y. Huang, T. Coleman, J. A. Rogers, *Science* **2011**, *333*, 838.
[34] S. Liu, D. S. Yang, S. Wang, H. Luan, Y. Sekine, J. B. Model, A. J. Aranyosi, R. Ghaffari, J. A. Rogers, *EcoMat* **2023**, *5*, e12270.
[35] R. L. Whistler, in *Industrial Gums*, 3rd ed., (Eds.: R. L. Whistler, J. N. Bemiller), Academic Press, London **1993**, pp. 309–339.
[36] Y. Ma, B. Zhang, I. Frenkel, Z. Zhang, X. Pei, F. Zhou, X. He, in *Progress in Adhesion and Adhesives*, John Wiley & Sons, Ltd, Hoboken, **2021**, pp. 739.
[37] L. Ge, S. Sethi, L. Ci, P. M. Ajayan, A. Dhinojwala, *Proc. Natl. Acad. Sci. U. S. A.* **2007**, *104*, 10792.
[38] Geday, Kaminsky, Lewis, Glazer, *J. Microsc.* **2000**, *198*, 1.
[39] J. Santander, T. Martin, A. Loh, C. Pohlenz, D. M. Gatlin, R. Curtiss, *Microbiology (Reading)* **2013**, *159*, 1471.